Communications Biology

https://doi.org/10.1038/s42003-026-09738-0

Article in Press

# Early life adversity impairs visually evoked innate defensive behaviors via oxytocin signaling

Received: 27 August 2025

Accepted: 10 February 2026

Cite this article as: Tan, H., Su, J., Ma, S. *et al.* Early life adversity impairs visually evoked innate defensive behaviors via oxytocin signaling. *Commun Biol* (2026). https://doi.org/10.1038/s42003-026-09738-0

Huiying Tan, Junying Su, Shaohua Ma, Shanping Chen, Qingqing Liu, Xing Yang & Liping Wang

# Early Life Adversity Impairs Visually Evoked Innate Defensive Behaviors via Oxytocin Signaling

Huiying Tan,[1,2,3] Junying Su,[1,2] Shaohua Ma,[1,2] Shanping Chen,[1,2] Qingqing Liu,[1,2] Xing Yang,[1,2] Liping Wang[1,2,3*]

1. CAS Key Laboratory of Brain Connectome and Manipulation, Shenzhen-Hong Kong Institute of Brain Science, Shenzhen Institute of Advanced Technology, Chinese Academy of Sciences, Shenzhen 518055, China
2. Guangdong Provincial Key Laboratory of Brain Connectome and Behavior, Brain Cognition and Brain Disease Institute, Shenzhen Institute of Advanced Technology, Chinese Academy of Sciences, Shenzhen 518055, China
3. University of Chinese Academy of Sciences, Beijing 10049, China

*Corresponding author: Liping Wang, Brain Cognition and Brain Disease Institute, Shenzhen Institute of Advanced Technology, Chinese Academy of Sciences, Shenzhen, China. E-mail: lp.wang@siat.ac.cn



## ABSTRACT

Recent studies have shown that ELA disrupts conditional fear behavior in mice; however, whether ELA affects innate fear behavior remains largely unknown. Here, we report that ELA induced by social deprivation on postnatal days 10–20 impairs looming-evoked innate defensive behaviors via an oxytocin (OT) signaling deficit. ELA leads to decreased OT receptor mRNA levels in the intermediate and deep layers of the superior colliculus (IDSC), and knockdown of this receptor in the superior colliculus mimics the defensive behavior deficit induced by ELA. OT neurons in the paraventricular nucleus of the hypothalamus modulate looming-evoked innate defensive behavior through projections to the IDSC. Moreover, intranasal OT ameliorated ELA-induced deficits in

defensive behavior. This study provides a theoretical basis for understanding how ELA induces a fear processing deficit that contributes to psychopathological outcomes and represents an initial step toward identifying potential treatment strategies.

## INTRODUCTION

Maintaining appropriate innate fear responses to threatening stimuli or signals is crucial for survival. Numerous clinical and animal studies have suggested that early life adversity (ELA) is associated with a range of negative psychopathological outcomes in adulthood[1-3]. Individuals who report ELA have a higher probability of accidental injuries, such as falls[4,5], brain injuries[6], car crashes, and burns[7], than individuals who report no childhood adversity. This reflects dysfunction in threat detection and response, indicative of inefficient innate fear processing. Accumulating evidence suggests that ELA alters neural architecture involved in threat detection and fear regulation[2,8,9]. Recent rodent studies have revealed that ELA impairs conditional fear behavior[10,11]; however, the effect of ELA on innate fear processing remains unknown.

Visual information is the primary sensory input for both animals and humans. A looming visual stimulus that mimics aerial predators has been used as an experimental paradigm to evoke innate defensive behavior and to study the neuronal mechanisms underlying innate fear processing across species[12-18]. Neuronal circuitry studies from our laboratory and others have revealed that the superior colliculus (SC), a layered midbrain structure, mediates looming-evoked innate defensive behavior in mice[19-24]. We previously reported that stress accelerates looming-evoked innate defensive behavior, mediated by a locus coeruleus to SC neural pathway, suggesting that this behavior can be modulated by changes in brain states in adulthood[25]. However, how early life stressors affect looming-evoked innate defensive behavior and whether the SC is involved require

further investigation.

Both human and rodent studies indicate that oxytocin (OT) signaling is down regulated in individuals who have experienced ELA[26-29]. In humans, lower blood OT levels and higher methylation of the OT receptor (*Oxtr*) gene have been detected in individuals reporting ELA[26,27]. In rodents, decreased OT immunoreactivity and decreased OXTR expression in the brain have been observed following ELA[28,29]. These findings suggest that OT signaling may be involved in the adverse neural outcomes following ELA. In mice, OT is primarily synthesized in the paraventricular nucleus of the hypothalamus (PVN) and the supraoptic nucleus (SON)[30]. OT neurons in the PVN flexibly modulate, via projections to relevant brain areas, the processing of a diverse range of fear behaviors, such as conditional fear retrieval[31-33], observational fear[34], and social fear during lactation[35]. Neural circuit tracing studies have shown that OT neurons in the PVN send projections directly to the intermediate and deep layers of the SC (IDSC, motor-related layers)[36,37]. Whether OT signaling in the PVN–IDSC pathway modulates looming-evoked innate defensive behaviors remains unknown.

Here, we report that ELA impairs looming-evoked innate defensive behaviors. ELA decreases *Oxtr* mRNA levels in the IDSC, disrupts the neural circuit from PVN OT neurons to the IDSC, and ultimately leads to a deficit in defensive behavior. Intranasal OT ameliorates ELA-induced defensive behavior deficits. This study provides insight into the pathology of psychological disorders that develop following ELA and paves the way for identifying potential therapeutic strategies.

**RESULTS**

**Late social deprivation impairs looming-evoked innate defensive behavior in adulthood**

We began by determining whether ELA affected looming-evoked innate defensive behaviors. Previous research has shown that different time windows of exposure to ELA have different effects on behavior and neural circuits in adulthood[38]. Therefore, we adopted a social deprivation paradigm and used two time periods—early social deprivation (ESD, postnatal days [PND] 1–12) and late social deprivation (LSD, PND 10–20)—to induce ELA in C57BL/6J mice (Fig. 1a). We then recorded looming-evoked innate defensive flight-to-refuge behavior at PND 60 using an automatic infrared behavior-monitor system developed by our group[39,40] (Fig. 1a). LSD mice took longer to return to the refuge (Fig. 1i), had longer trajectories (Fig. 1j–k), exhibited slower return speeds (Fig. 1l–n), and spent less time in the refuge after each looming trial (Fig. 1o) compared with control mice, indicating diminished innate defensive responses. In contrast, no significant differences were observed between ESD and control mice (Fig. 1b–h). These data demonstrate that looming-evoked innate defensive behavior is impaired in adult LSD mice but not in ESD mice.

Our previous research demonstrated that looming-evoked innate defensive behavior remains highly conserved throughout the lifespan in males and females[41]. To investigate potential sex-specific differences, we analyzed the behavioral responses of male and female LSD mice to looming stimuli separately, but found no significant differences (Supplementary Fig. 1). To exclude the effects of motor function and physical developmental differences on defensive behavior, we recorded mean speed (Supplementary Fig. 2a) and shelter ratio (Supplementary Fig. 2b) during habituation to the looming test, as well as body weight (Supplementary Fig. 2c) at PND

7, 14, 21, 30, and 60. No significant differences were observed between the LSD and control groups. Previous work from our group revealed that anxiety states in mice influence looming-evoked defensive responses[25]. Therefore, we evaluated LSD mice in an open-field test (Supplementary Fig. 2d–g) and an elevated plus maze (Supplementary Fig. 2h–k). The results indicated that LSD did not affect anxiety levels in mice.

**LSD mice have lower *Oxtr* mRNA expression in the IDSC**

The SC is fundamental in mediating looming-evoked innate defensive behavior[42]. Downregulation of OT signaling has been documented following ELA[26-29]. Additionally, single-neuron projectome analyses have demonstrated that PVN OT neurons project to the IDSC[37]. Thus, we employed fluorescence *in situ* hybridization (FISH) to co-stain SC neurons for *c-fos* and *Oxtr* mRNA expression after the looming test (Supplementary Fig. 3a). Most *c-fos* positive neurons induced by looming stimuli expressed *Oxtr* in the IDSC (intermediate layer [IL]: 58.55%; deep layer [DL]: 56.04%; Supplementary Fig. 3b, 3c), but not in the superficial layer (SL). This observation highlighted the potential involvement of OT signaling in the IDSC in the context of LSD-induced deficits in innate defensive behavior.

To investigate whether OT signaling contributes to the observed innate defensive behavior deficits, we quantified OT neurons (Fig. 2a–b) and measured OT release in the PVN and SON (Fig. 2c), and OT release in the SC (Fig. 2d) of LSD mice. No significant differences emerged between the LSD and control groups. Subsequently, we assessed *Oxtr* expression levels in the IDSC of LSD

mice. FISH analysis revealed a reduction in *c-fos*$^{+}$ cells (Fig. 2e–f), decreased density of *Oxtr*$^{+}$ cells (Fig. 2g), and diminished mean intensity of *Oxtr* within *c-fos*$^{+}$ cells in the IDSC of LSD mice (Fig. 2h). Collectively, these results suggest that the innate defensive behavior deficit induced by LSD may be mediated by reduced *Oxtr* expression in the IDSC.

**_Oxtr_ knockdown in the SC mimics the innate defensive behavior deficit induced by LSD**

Next, we knocked down *Oxtr* in the SC and recorded looming-evoked flight-to-refuge behavior. We injected AAV-hSyn-iCre-GFP bilaterally into the SC of Oxtr$^{flox}$ mice (Fig. 3a). Knockdown efficiency was confirmed by GFP expression (Fig. 3b), and protein levels were measured by western blot analysis (Fig. 3c and Supplementary Fig. 4). Compared with wild-type (-/-) mice, homozygous (+/+) Oxtr$^{flox}$ mice took a longer time to return to the refuge (Fig. 3d), had longer trajectories (Fig. 3e–f), slower return speeds (Fig. 3g–i), and spent less time in the refuge after each looming trial (Fig. 3j). These findings indicate that SC *Oxtr* knockdown mice and LSD mice display similar deficits in looming-evoked defensive behavior.

**Activation of oxytocinergic terminals in the IDSC enhances innate defensive behavior**

To further investigate how OT signaling in the IDSC regulates innate defensive behavior, we activated oxytocinergic terminals using an optogenetic approach and assessed behavioral responses to the looming stimulus. We injected an AAV carrying hSyn-DIO-ChR2-mCherry into the PVN of OT-Cre mice (Fig. 4a). After viral expression (Fig. 4b) and bilateral implantation of optic fibers (Fig. 4c), the mice received 473-nm blue light stimulation (pulse duration 10 ms, 30

Hz, 10–20 mW) throughout the entire looming test session. Compared with the mCherry control group, the ChR2 group showed enhanced responses to the looming stimulus, with shorter latency to refuge (Fig. 4d), faster return speeds (Fig. 4g–i), and more time spent in the refuge after looming (Fig. 4J). These results indicate that PVN OT neurons modulate looming-evoked innate defensive behaviors via projections to the IDSC.

**Intranasal OT ameliorates the innate defensive behavior deficit induced by LSD**

Intranasal OT administration has been shown to reach multiple brain regions and upregulate OXTR expression, making it a promising potential therapeutic approach[43-45]. To determine whether OT administration could rescue the LSD-induced deficit in innate defensive behavior, we treated LSD mice with intranasal OT on PND 48–60, every other day (seven days in total, 20 μg $kg^{-1}$ body weight each time)[46,47], followed by the looming test. The deficit in innate defensive behavior induced by LSD was partially rescued (Fig. 5). Compared with the saline-treated LSD mice, the OT-treated LSD mice had faster mean return speeds (Fig. 5e) and spent more time in the refuge after looming (Fig. 5g).



**DISCUSSION**

This study demonstrated that ELA impairs looming-evoked flight-to-refuge innate defensive behavior via an OT signaling deficit. ELA induced by social deprivation on PND 10–20 diminished defensive behavior in adult mice. ELA led to decreased in *Oxtr* mRNA expression in the IDSC and a deficit in defensive behavior. Knockdown of OXTR in the SC mimicked the behavioral deficits

caused by ELA in mice. OT neurons in the PVN modulated defensive behavior via projections to the IDSC. Intranasal OT ameliorated ELA-induced deficits in defensive behavior.

There is consensus that ELA has negative effects on neuronal circuitry[2,8,48,49]. ELA alters brain maturation and negatively affects the development of sensory processing and architecture involved in threat detection and fear behaviors[2,8,9]. ELA models in rodents have been used to elucidate the underlying neural mechanisms. Maternal separation or limited bedding models before weaning are the most frequently used approaches to induce ELA[50]. Specifically, limited bedding models that induce ELA impair conditional fear memory by reducing hippocampal synaptic plasticity[10] and preadolescent conditional fear expression by accelerating parvalbumin-positive cell development in the basolateral amygdala[11]. Maternal separation with early weaning induces visual dysfunction and retinal structural alterations, and looming behavior deficits in adult mice[51]. However, the effects of ELA on brain circuits involved in innate defensive behavior remain largely unknown. Our study adopted a social deprivation paradigm to induce ELA, which involved the manipulation of normal maternal care and led to family dysfunction. We found that social deprivation from PND 10–20 reduced *Oxtr* mRNA expression in the IDSC and impaired looming-evoked innate defensive behavior in adult mice. Our findings represent an important advancement in understanding how ELA induces innate defensive behavior deficits.

Maternal nursing plays a vital role in offspring brain development, particularly during sensitive periods[52,53]. Maternal absence from the nest regulated the brain state of the offspring during PND 12-19[54]. Meanwhile, maternal separation between PND 10 and 20 increases

susceptibility to depression-like behavior, whereas same separation from PND 2 to 12 did not[38]. Furthermore, OXTR expression follows a specific phased pattern during postnatal development: it begins to increase from PND 7 and reaches adult levels by PND 21[55,56]. Building on these observations, we conducted social deprivation experiments during PND 1–12 and PND 10–20. Our results indicated that social deprivation from PND 10 to 20, but not from PND 1 to 12 impaired looming-evoked innate defensive behavior through an OXTR deficit in the IDSC. This suggests that maternal nursing during PND 10–20 is particularly important for the development of OT signaling and represents a critical period for regulating innate defensive behavior.

A large body of animal model literature has documented the involvement of OT signaling in modulating of various types of fear behavior, including conditional fear[31-33], observational fear[34], and social fear[35,57]. For example, during conditional fear retrieval, PVN OT neurons become activated, release OT to terminals in the central amygdala (CeA), and suppress freezing behavior by acting on GABAergic neurons in the CeA[32]. Likewise, chemogenetic activation of PVN OT neurons enhances observational fear in unfamiliar mice[34], and OT signaling in the lateral septum attenuates social fear expression in female mice during lactation[35]. OT signaling in the CeA of rat dams suppresses fear levels and self-defense responses, allowing mothers to protect their offspring when danger stimuli are present[57]. OT neurons in the medioventral bed nucleus of the stria terminalis drive stress-induced social vigilance and avoidance[58]. These studies suggest that OT signaling flexibly modulates fear behavior in response to physiological and contextual factors. Our study demonstrated that activation of oxytocinergic terminals in the IDSC accelerated looming

responses. These findings expand the current knowledge on the modulation of fear behavior by OT signaling.

Both clinical and animal studies have shown that ELA is a high risk factor for mental disorders[8] and that OT signaling is involved in the development of these disorders[29,50]. Populations with mental disorders after ELA exhibits deficit responses to fearful facial expressions[59] or threat stimuli[60]. Our findings align with this, showing that ELA impairs innate defensive behavior through an OT signaling deficit in the IDSC. Intranasal OT ameliorated the behavioral deficits induced by ELA. OT has been used as an intervention for mental disorders such as depression[61] and schizophrenia[62,63]. However, the reported outcomes are controversial, as some clinical studies indicate that intranasal OT improves symptoms[61,64] while others suggest no significant effect[63,65]. Therefore, the mechanism of intranasal OT warrants further investigation to improve understanding of the basic OT signaling theory. Additionally, clinical trials should be conducted with greater precision and include comprehensive analyses of non-significant results[66,67]. Further research on the connection between mental disorders and innate defensive behavior may clarify the development and early treatment of these conditions. Intranasally administered labeled OT reportedly reaches the brain in rhesus macaques[43], with affected areas exhibiting higher OXTR expression in human[44]. Although our experiment did not directly show increased OT levels or OXTR expression in the IDSC, we posit that intranasal OT enhances PVN–IDSC OT signaling, thereby ameliorating the LSD-induced innate defensive behavior deficit. Cumulatively, this study has clarified the neural mechanism by which OT signaling mediates visually evoked innate

defensive behavior after ELA. This provides a theoretical foundation for understanding OT's role in mental illnesses linked to ELA and marks an initial step toward developing potential treatment strategies.

## METHODS

### Animals

C57BL/6J mice (Beijing Vital River Laboratory Animal Technology, Beijing, China), OT-Cre mice (Jackson Laboratory), and $Oxtr^{flox}$ mice (Jackson Laboratory) were used in this study. Mice were housed at 22–25 °C in a 12-h light/dark cycle environment with *ad libitum* access to food and water. All husbandry and experimental procedures have been approved by the Animal Care and Use Committees at the Shenzhen Institute of Advanced Technology, Chinese Academy of Sciences. We have complied with all relevant ethical regulations for animal use.



The experimental unit is a single animal. Animals were randomly assigned to experimental conditions using the random number process in MATLAB (MathWorks, USA). During the experiment, mice from the control and treatment groups were alternately tested. All mice were maintained in the same room on the same rack to reduce potential confounding factors. Except for the social deprivation procedures, all the other experiments were performed when the mice were 8 to 12 weeks old. Male and female mice were used in approximately equal numbers. The specific numbers of male and female animals used in each experiment have been listed in Supplementary data 1. In order to alleviate the suffering of animals, mice were anesthetized with an intraperitoneal

injection of sodium pentobarbital (80 mg kg-1 bodyweight) and placed over a heating blanket throughout the surgical and recovery periods. Postoperative recovery was monitored at 10 min intervals. If a mouse is found to be in poor or moribund condition following surgery, it will be humanely euthanized via carbon dioxide inhalation as assessed by the veterinarian.

**Social deprivation procedures**

The social deprivation paradigm used in this study was based on procedures modified from previous work[38,68]. Pregnant C57BL/6J mice were housed separately from day 14 of pregnancy and randomly assigned to control or social deprivation groups. Pups were separated from their dams and littermates for 3 h per day. For ESD, this occurred from PND 1 to 12, and for LSD, from PND 10 to 20. The isolation periods occurred at different times each day within the light cycle (8:00 a.m. to 8:00 p.m.). During separation, pups were placed individually in a 10 × 10 ×10 $cm^3$ chamber with clean bedding and kept in an incubator at 30 ± 1 °C. After separation, pups were reunited with their dams and littermates. Pups in the control group remained undisturbed in the nests with their dams and littermates. All pups were weaned on PND 21 and housed in groups of three to five same-sex littermates.

**Looming test**

The looming test was performed using an automatic infrared behavior-monitor system developed by our group[39,40]. Briefly, the system comprised three parts: (i) a monitor to display the looming stimuli, (ii) a circular open-field arena adjacent to a narrow alley that served as a refuge, and (iii)

an infrared touchscreen frame used to record mouse trajectories in real time. Each mouse was habituated to the arena for 5 min and allowed to automatically trigger a maximum of 3 looming stimulus trials in 20 min by stopping at the center of the open field. There was a minimum of 3 min between each looming stimulus presentation. The visual looming stimulus was generated by MATLAB and consisted of a black expanding disc on the screen that changed from a visual angle of 2° to 40° within 250 ms, remained at 40° for 50 ms, and then repeated the 2° to 40° change 15 times with a 30 ms interval between iterations.

**Open-field test**

Mice were individually placed in an open-field arena (50 × 50 ×50 $cm^3$) and allowed to move freely for 5 min. An unmarked, smaller concentric square (25 × 25 $cm^2$) inside the arena was defined as the arena center. The movement of each mouse was monitored with a video camera and analyzed using Anymaze software (Stoelting, IL, USA).

**Elevated plus maze**

Mice were individually placed in the center of a four-arm plus maze with two open arms and two closed arms elevated 50 cm above the ground for 5 min. Movement was monitored using a video camera and analyzed using Anymaze software.

**Immunofluorescence staining**

Mice were deeply anesthetized with an intraperitoneal injection of sodium pentobarbital (100 mg

kg$^{-1}$ body weight) and transcardially perfused with cold phosphate-buffered saline (PBS), followed by 4% paraformaldehyde (PFA, Boster, China). Brains were fixed in 4% PFA at 4 °C overnight, then transferred to 30% sucrose for 2 days at 4 °C to equilibrate. Coronal brain sections were cut at 30 μm thickness on a cryostat microtome (Leica CM1950, Germany), washed in PBS three times for 10 min each, and permeabilized in a blocking solution containing 0.3% Triton X-100 and 10% goat serum for 1 h at room temperature. Sections were then incubated overnight at 4 °C with anti-OT antibody (Cat#AB911, 1:500, Millipore, USA). After gentle rinsing in PBS (3 × 10 min), the sections were incubated with a secondary antibody (Alexa Fluor 488, 1:200, Jackson ImmunoResearch, USA) for 1 h at room temperature and rinsed again in PBS (3 × 10 min). Sections were mounted in medium containing DAPI (Vector Laboratories, Burlingame, CA, USA) and gently cover-slipped. Imaging was performed using confocal microscopy (LMS880, Zeiss, Germany), and OT-positive neurons were counted using ImageJ (National Institutes of Health, Bethesda, MD, USA).



**OT peptide release measurement**

OT release from the PVN and SON was measured as previously described[69]. Briefly, the mice were deeply anesthetized with an intraperitoneal injection of sodium pentobarbital (100 mg/kg bodyweight), and their brains were rapidly removed. Coronal sections of the ventral medial region containing the PVN and SON were cut with a vibratome (VT1200, Leica, Germany) in oxygenated ice-cold choline chloride solution, followed by 30 min incubation in artificial cerebro spinal fluid (ACSF) at 37 °C. Sections were then placed in a 48-well cell culture plate with 150 μL ACSF at

28 °C. Samples were collected every 5 min for 20 min after secretion reached equilibrium. OT concentration was measured using an ELISA kit (Cat#ADI-900-153A-0001, ENZO, USA), according to the manufacturer's instructions.

**FISH**

Mice were transcardially perfused with 4% PFA. After overnight fixation at 4 °C, brains were equilibrated in 30% sucrose for 2 days at 4 °C. Coronal brain sections were cut at an 18 μm thickness using a cryostat microtome, mounted on Superfrost Ultra Plus slides (Cat#4951PLUS-001E, Thermo Scientific, USA), and store at -80 °C. Sections were processed according to the manufacturer's protocol using the RNAscope Multiplex Fluorescent Reagent Kit v2 (Cat#323100, Advanced Cell Diagnostics, USA). Positive (1:100, Cat#321651, Advanced Cell Diagnostics, USA) and a negative (1:100, Cat#320871, Advanced Cell Diagnostics, USA) control probes were employed to validate in the brain sections to eliminate the risk of nonspecific probe binding.



Initially, sections were dried at 39 °C for 2 h, washed with 1‰ diethyl pyrocarbonate (DEPC)-treated PBS, incubated in 3% hydrogen peroxide diluted in methanol for 5 min, and transferred to the target buffer at 100 °C for 15 min. After washing twice with 1‰ DEPC-treated water, the sections were incubated in anhydrous ethanol for 1 min and subsequently dried at room temperature. Protease treatment was applied for 15 min at 40 °C, followed by hybridization with a mixture containing *c-fos* (1:100, Cat#1310761-C2, Advanced Cell Diagnostics, USA) and *Oxtr* (1:50, Cat#412171-C3, Advanced Cell Diagnostics, USA) probes for 2 h at 40 °C. Next,

amplification buffer was added to each channel for 30 min at 40 °C followed by horseradish peroxidase for 15 min at 40 °C and TSA Plus fluorescent dyes for 30 min at 40 °C. For *c-fos* staining, fluorescein tyramide dye (1:200, Cat# K1084-1, APExBIO, USA) was used, while cyanine 3 tyramide dye (1:200, Cat# K1085-1, APExBIO, USA) was used for *Oxtr* staining. Finally, the sections were incubated in 1‰ DEPC-treated PBS with DAPI (1:5000, Cat#4083S, Cell Signaling Technology, USA).

Imaging was performed using a virtual microscopy slide-scanning system (VS120, Olympus, Japan), and quantification of fluorescently positive cells was performed with ImageJ. High-magnification images were acquired via confocal microscopy (LSM 980, ZEISS, Germany). Mean intensity values for *Oxtr* within *c-fos*$^+$ cells were assessed using ZEN software (Blue edition 3.6, ZEISS). Cell types were identified based on *c-fos* and DAPI staining. Regions of interest were manually delineated according to DAPI staining to avoid false positive signals. For intensity mean value statistics, 60 cells per mouse were randomly selected. Twenty images per mouse were captured. All *Oxtr* and *c-fos* double-positive cells were annotated. Cells included in statistical analyses were selected via a random number process.



**Virus injection**

Viruses were administered to mice at eight weeks of age, as previously described[70], and behavior tests were performed four weeks post injection. In brief, AAV-hSyn-iCre-GFP (Liping Wang's Lab at the CAS), AAV-hSyn-DIO-mCherry (Taitool, China), and AAV-hSyn-DIO-ChR2-mCherry

(Taitool, China) were used. Mice were anesthetized with an intraperitoneal injection of sodium pentobarbital (80 mg $kg^{-1}$ bodyweight) and placed in a stereotaxic apparatus (RWD, China). Above the target region coordinates, the skull was thinned with a dental drill and carefully removed. Virus injections were performed using a 33-gauge metal needle (Hamilton, USA) attached to a 10 μL syringe, which was connected to a microsyringe pump (UMP3/Micro4, USA). The PVN (total volume of 200 nL) coordinates were: AP, -0.90 mm, ML, ±0.25 mm and DV, -4.80 mm. The SC (total volume of 300 nL) coordinates were: AP, -3.85 mm, ML, ±0.80 mm and DV, -1.80 mm. The expression of the virus was confirmed by tissue sections. Animals without virus expression were not included in the statistics.

**Western blot analysis**

Mice were anesthetized using isoflurane. The brains were rapidly removed and placed in a mouse brain mold (RWD, China) and incubated in cold PBS. Brains were sectioned into 1 mm coronal slices, and the SC region was dissected under a microscope. Dissected SC tissues were lysed in RIPA lysis buffer (Cat#89900, Thermo Scientific, USA) containing protease inhibitor (100:1, Cat#87786, Thermo Scientific, USA), utilizing an ultrasonic cell lysis instrument. Next, 20 μg of each sample, prepared with sample loading buffer (Cat# E151-05, GenStar, China), was loaded onto 10% polyacrylamide gels (Cat# E159-10, GenStar, China), and electrophoretically transferred to polyvinylidene difluoride (PVDF) membranes (Cat# ISEQ00010, Millipore, USA). The membranes were incubated with rabbit anti-Oxtr (1:1000, Cat# 23045-1-AP, Proteintech, USA) and mouse anti-GAPDH (1:2000, Cat# AC002, ABclonal, China) primary antibodies overnight at

4 °C, washed thrice with tris-buffered saline-tween (TBST), and incubated with goat anti-rabbit IgG H&L (1:2000, Cat# bs-0295G-HRP, Bioss, China) and goat anti-mouse IgG H&L (1:2000, Cat# bs-0296G-HRP, Bioss, China) HRP-conjugated secondary antibodies for 1 h at room temperature. Following three additional washes with TBST, fluorescence signals were detected using the SuperSignal West Pico PLUS Chemiluminescent Substrate kit (Cat# 34580, Thermo Scientific, USA) and visualized with a gel imaging system (Amersham ImageQuant 800, Cytiva, Sweden). Images were analyzed using ImageJ.

### *In vivo* optogenetic manipulation

AAV encoding hSyn-DIO-ChR2-mCherry was bilaterally injected into the PVN of OT-Cre mice. AAV-hSyn-DIO-mCherry was used as the control. After three weeks of viral expression, optic fibers (NA: 0.37; Inper, China) were bilaterally implanted into the SC (AP: -3.85 mm, ML: ±1.20 mm, DV: -1.50 mm) at a 15 ° angle from the vertical axis[71]. The optical fibers were fixed using dental cement. After one week of recovery, optogenetic manipulation was performed using a 473-nm blue laser (Newdoon, China). Mice received 473-nm light stimulation (10-ms pulse duration, 30 Hz, 10-20 mW) from the beginning to the end of the looming test. The position of the optical fiber implantation was confirmed by tissue sectioning. Animals with inaccurate fiber implantation were not included in the statistics.

### OT administration

OT (Cat#P1029, Selleckchem, USA) was dissolved in sterile saline (100 mg $mL^{-1}$), aliquoted, and

stored at -80 °C. Prior to use, OT was diluted in sterile saline to prepare a working solution of 20 μg $kg^{-1}$ (5 μL per mouse), adjusted according to each animal's weight. OT was administered as previously described[72]. Mice were briefly anesthetized with isoflurane and held in a supine position. The OT solution was added dropwise bilaterally (2.5 μL per nostril) and evenly distributed over the rhinarium's squamous epithelium using the rounded tip of a micropipette. After administration, mice remained supine for 1 min to prevent reflux of the solution. OT was administered every other day between PND 48 and 60 for a total of seven sessions[46,47]. Looming tests were conducted 30 min after OT administration on PND 60. The saline control group underwent an identical anesthesia protocol and intranasal administration procedure.

**Statistics and Reproducibility**

Looming behavior data were analyzed using MATLAB, and each trial was included in the statistical analysis, with graphical representation in a box plot. Other data were analyzed in GraphPad Prism 10.0 (GraphPad, USA). Two-group comparisons used unpaired two-tailed Student's *t*-tests or Mann-Whitney U-test. Data are presented as mean ± standard error of the mean (SEM). A $p < 0.05$ was considered statistically significant. The sample sizes were provided in the figure legends, consistent with numerous analogous experimental studies in the field. All experiments were independently repeated at least three times to ensure consistency of results. The experimental execution and data analysis were carried out by different investigators to eliminate any subjective influence. Investigators were blinded to group allocation during data collection and analysis.

## Data availability

Original full blots (Supplementary Fig. 4) and the numerical source data for graphs and charts (Supplementary data 1) have been submitted as supplementary information.

## Code availability

No new custom code was generated for this manuscript.

## REFERENCES


1. Felitti, V.J., Anda, R.F., Nordenberg, D., Williamson, D.F., Spitz, A.M., Edwards, V., Koss, M.P., and Marks, J.S. (1998). Relationship of childhood abuse and household dysfunction to many of the leading causes of death in adults. The Adverse Childhood Experiences (ACE) Study. Am J Prev Med *14*, 245-258. 10.1016/s0749-3797(98)00017-8.
2. Teicher, M.H., Samson, J.A., Anderson, C.M., and Ohashi, K. (2016). The effects of childhood maltreatment on brain structure, function and connectivity. Nat Rev Neurosci *17*, 652-666. 10.1038/nrn.2016.111.
3. Bhutta, Z.A., Bhavnani, S., Betancourt, T.S., Tomlinson, M., and Patel, V. (2023). Adverse childhood experiences and lifelong health. Nature Medicine *29*, 1639-1648. 10.1038/s41591-023-02426-0.
4. Huang, R., Li, S., Hu, J., Ren, R., Ma, C., Peng, Y., and Wang, D. (2024). Adverse childhood experiences and falls in older adults: The mediating role of depression. Journal of Affective Disorders *365*, 87-94. 10.1016/j.jad.2024.08.080.
5. Tan, H., Liu, M., Ren, H., Zhou, J., Guo, Y., and Jiang, X. (2025). Associations of Adverse Childhood Experiences With Falls and Fall Risk Factors Among Middle-Aged and Older Adults in China. American Journal of Preventive Medicine *68*, 998-1009. 10.1016/j.amepre.2025.02.006.
6. Guinn, A.S., Ports, K.A., Ford, D.C., Breiding, M., and Merrick, M.T. (2019). Associations between adverse childhood experiences and acquired brain injury, including traumatic brain injuries, among adults: 2014 BRFSS North Carolina. Inj Prev *25*, 514-520. 10.1136/injuryprev-2018-042927.
7. Ford, K., Hughes, K., Cresswell, K., Griffith, N., and Bellis, M.A. (2022). Associations between Adverse Childhood Experiences (ACEs) and Lifetime Experience of Car Crashes and Burns: A Cross-Sectional Study. International journal of environmental research and public health *19*. 10.3390/ijerph192316036.
8. Short, A.K., and Baram, T.Z. (2019). Early-life adversity and neurological disease: age-old questions and novel answers. Nat Rev Neurol *15*, 657-669. 10.1038/s41582-019-0246-5.
9. Murthy, S., and Gould, E. (2020). How Early Life Adversity Influences Defensive Circuitry. Trends Neurosci *43*, 200-212. 10.1016/j.tins.2020.02.001.

10. Lesuis, S.L., Lucassen, P.J., and Krugers, H.J. (2019). Early life stress impairs fear memory and synaptic plasticity; a potential role for GluN2B. Neuropharmacology *149*, 195-203. 10.1016/j.neuropharm.2019.01.010.
11. Manzano Nieves, G., Bravo, M., Baskoylu, S., and Bath, K.G. (2020). Early life adversity decreases pre-adolescent fear expression by accelerating amygdala PV cell development. Elife *9*. 10.7554/eLife.55263.
12. Schiff, W., Caviness, J.A., and Gibson, J.J. (1962). Persistent fear responses in rhesus monkeys to the optical stimulus of "looming". Science *136*, 982-983. 10.1126/science.136.3520.982.
13. Ball, W., and Tronick, E. (1971). Infant responses to impending collision: optical and real. Science *171*, 818-820. 10.1126/science.171.3973.818.
14. Yilmaz, M., and Meister, M. (2013). Rapid innate defensive responses of mice to looming visual stimuli. Curr Biol *23*, 2011-2015. 10.1016/j.cub.2013.08.015.
15. Temizer, I., Donovan, J.C., Baier, H., and Semmelhack, J.L. (2015). A Visual Pathway for Looming-Evoked Escape in Larval Zebrafish. Curr Biol *25*, 1823-1834. 10.1016/j.cub.2015.06.002.
16. Perez-Fernandez, J., Kardamakis, A.A., Suzuki, D.G., Robertson, B., and Grillner, S. (2017). Direct Dopaminergic Projections from the SNc Modulate Visuomotor Transformation in the Lamprey Tectum. Neuron *96*, 910-924 e915. 10.1016/j.neuron.2017.09.051.
17. Ache, J.M., Polsky, J., Alghailani, S., Parekh, R., Breads, P., Peek, M.Y., Bock, D.D., von Reyn, C.R., and Card, G.M. (2019). Neural Basis for Looming Size and Velocity Encoding in the Drosophila Giant Fiber Escape Pathway. Curr Biol *29*, 1073-1081 e1074. 10.1016/j.cub.2019.01.079.
18. Clery, J.C., Schaeffer, D.J., Hori, Y., Gilbert, K.M., Hayrynen, L.K., Gati, J.S., Menon, R.S., and Everling, S. (2020). Looming and receding visual networks in awake marmosets investigated with fMRI. Neuroimage *215*, 116815. 10.1016/j.neuroimage.2020.116815.
19. Shang, C., Liu, Z., Chen, Z., Shi, Y., Wang, Q., Liu, S., Li, D., and Cao, P. (2015). BRAIN CIRCUITS. A parvalbumin-positive excitatory visual pathway to trigger fear responses in mice. Science *348*, 1472-1477. 10.1126/science.aaa8694.
20. Shang, C., Chen, Z., Liu, A., Li, Y., Zhang, J., Qu, B., Yan, F., Zhang, Y., Liu, W., Liu, Z., et al. (2018). Divergent midbrain circuits orchestrate escape and freezing responses to looming stimuli in mice. Nat Commun *9*, 1232. 10.1038/s41467-018-03580-7.
21. Evans, D.A., Stempel, A.V., Vale, R., Ruehle, S., Lefler, Y., and Branco, T. (2018). A synaptic threshold mechanism for computing escape decisions. Nature *558*, 590-594. 10.1038/s41586-018-0244-6.
22. Zhou, Z., Liu, X., Chen, S., Zhang, Z., Liu, Y., Montardy, Q., Tang, Y., Wei, P., Liu, N., Li, L., et al. (2019). A VTA GABAergic Neural Circuit Mediates Visually Evoked Innate Defensive Responses. Neuron. 10.1016/j.neuron.2019.05.027.
23. Wei, P., Liu, N., Zhang, Z., Liu, X., Tang, Y., He, X., Wu, B., Zhou, Z., Liu, Y., Li, J., et al. (2015). Processing of visually evoked innate fear by a non-canonical thalamic pathway. Nat Commun *6*, 6756. 10.1038/ncomms7756.
24. Liu, X., Lai, J., Han, C., Zhong, H., Huang, K., Liu, Y., Zhu, X., Wei, P., Tan, L., Xu, F., and Wang, L. (2025). Neural circuit underlying individual differences in visual escape habituation. Neuron. 10.1016/j.neuron.2025.04.018.
25. Li, L., Feng, X., Zhou, Z., Zhang, H., Shi, Q., Lei, Z., Shen, P., Yang, Q., Zhao, B., Chen, S., et al. (2018). Stress Accelerates Defensive Responses to Looming in Mice and Involves a Locus Coeruleus-Superior

Colliculus Projection. Curr Biol *28*, 859-871 e855. 10.1016/j.cub.2018.02.005.

26. Ebner, N.C., Lin, T., Muradoglu, M., Weir, D.H., Plasencia, G.M., Lillard, T.S., Pournajafi-Nazarloo, H., Cohen, R.A., Sue Carter, C., and Connelly, J.J. (2019). Associations between oxytocin receptor gene (OXTR) methylation, plasma oxytocin, and attachment across adulthood. Int J Psychophysiol *136*, 22-32. 10.1016/j.ijpsycho.2018.01.008.
27. Ellis, B.J., Horn, A.J., Carter, C.S., van, I.M.H., and Bakermans-Kranenburg, M.J. (2021). Developmental programming of oxytocin through variation in early-life stress: Four meta-analyses and a theoretical reinterpretation. Clin Psychol Rev *86*, 101985. 10.1016/j.cpr.2021.101985.
28. He, Z., Young, L., Ma, X.M., Guo, Q., Wang, L., Yang, Y., Luo, L., Yuan, W., Li, L., Zhang, J., et al. (2019). Increased anxiety and decreased sociability induced by paternal deprivation involve the PVN-PrL OTergic pathway. Elife *8*. 10.7554/eLife.44026.
29. Onaka, T., and Takayanagi, Y. (2021). The oxytocin system and early-life experience-dependent plastic changes. J Neuroendocrinol, e13049. 10.1111/jne.13049.
30. Jurek, B., and Neumann, I.D. (2018). The Oxytocin Receptor: From Intracellular Signaling to Behavior. Physiol Rev *98*, 1805-1908. 10.1152/physrev.00031.2017.
31. Viviani, D., Charlet, A., van den Burg, E., Robinet, C., Hurni, N., Abatis, M., Magara, F., and Stoop, R. (2011). Oxytocin selectively gates fear responses through distinct outputs from the central amygdala. Science *333*, 104-107. 10.1126/science.1201043.
32. Knobloch, H.S., Charlet, A., Hoffmann, L.C., Eliava, M., Khrulev, S., Cetin, A.H., Osten, P., Schwarz, M.K., Seeburg, P.H., Stoop, R., and Grinevich, V. (2012). Evoked axonal oxytocin release in the central amygdala attenuates fear response. Neuron *73*, 553-566. 10.1016/j.neuron.2011.11.030.
33. Hasan, M.T., Althammer, F., Silva da Gouveia, M., Goyon, S., Eliava, M., Lefevre, A., Kerspern, D., Schimmer, J., Raftogianni, A., Wahis, J., et al. (2019). A Fear Memory Engram and Its Plasticity in the Hypothalamic Oxytocin System. Neuron *103*, 133-146 e138. 10.1016/j.neuron.2019.04.029.
34. Pisansky, M.T., Hanson, L.R., Gottesman, II, and Gewirtz, J.C. (2017). Oxytocin enhances observational fear in mice. Nat Commun *8*, 2102. 10.1038/s41467-017-02279-5.
35. Menon, R., Grund, T., Zoicas, I., Althammer, F., Fiedler, D., Biermeier, V., Bosch, O.J., Hiraoka, Y., Nishimori, K., Eliava, M., et al. (2018). Oxytocin Signaling in the Lateral Septum Prevents Social Fear during Lactation. Curr Biol *28*, 1066-1078 e1066. 10.1016/j.cub.2018.02.044.
36. Son, S., Manjila, S.B., Newmaster, K.T., Wu, Y.-t., Vanselow, D.J., Ciarletta, M., Anthony, T.E., Cheng, K.C., and Kim, Y. (2022). Whole-Brain Wiring Diagram of Oxytocin System in Adult Mice. The Journal of Neuroscience, JN-RM-0307-0322. 10.1523/jneurosci.0307-22.2022.
37. Li, H., Jiang, T., An, S., Xu, M., Gou, L., Ren, B., Shi, X., Wang, X., Yan, J., Yuan, J., et al. (2024). Single-neuron projectomes of mouse paraventricular hypothalamic nucleus oxytocin neurons reveal mutually exclusive projection patterns. Neuron. 10.1016/j.neuron.2023.12.022.
38. Pena, C.J., Kronman, H.G., Walker, D.M., Cates, H.M., Bagot, R.C., Purushothaman, I., Issler, O., Loh, Y.E., Leong, T., Kiraly, D.D., et al. (2017). Early life stress confers lifelong stress susceptibility in mice via ventral tegmental area OTX2. Science *356*, 1185-1188. 10.1126/science.aan4491.
39. Yang, X., Liu, Q., Zhong, J., Song, R., Zhang, L., and Wang, L. (2020). A simple threat-detection strategy in mice. BMC Biol *18*, 93. 10.1186/s12915-020-00825-0.
40. Liu, Q., Yang, X., Song, R., Su, J., Luo, M., Zhong, J., and Wang, L. (2021). An Infrared Touch System for

Automatic Behavior Monitoring. Neurosci Bull *37*, 815-830. 10.1007/s12264-021-00661-4.

41. Liu, X., Feng, X., Huang, H., Huang, K., Xu, Y., Ye, S., Tseng, Y.T., Wei, P., Wang, L., and Wang, F. (2022). Male and female mice display consistent lifelong ability to address potential life-threatening cues using different post-threat coping strategies. BMC Biol *20*, 281. 10.1186/s12915-022-01486-x.
42. Lischinsky, J.E., and Lin, D. (2019). Looming Danger: Unraveling the Circuitry for Predator Threats. Trends Neurosci *42*, 841-842. 10.1016/j.tins.2019.10.004.
43. Lee, M.R., Shnitko, T.A., Blue, S.W., Kaucher, A.V., Winchell, A.J., Erikson, D.W., Grant, K.A., and Leggio, L. (2020). Labeled oxytocin administered via the intranasal route reaches the brain in rhesus macaques. Nat Commun *11*, 2783. 10.1038/s41467-020-15942-1.
44. Habets, P.C., McLain, C., and Meijer, O.C. (2021). Brain areas affected by intranasal oxytocin show higher oxytocin receptor expression. Eur J Neurosci. 10.1111/ejn.15447.
45. Moerkerke, M., Daniels, N., Tibermont, L., Tang, T., Evenepoel, M., Van der Donck, S., Debbaut, E., Prinsen, J., Chubar, V., Claes, S., et al. (2024). Chronic oxytocin administration stimulates the oxytocinergic system in children with autism. Nature Communications *15*. 10.1038/s41467-023-44334-4.
46. Joushi, S., Taherizadeh, Z., Esmaeilpour, K., and Sheibani, V. (2022). Environmental enrichment and intranasal oxytocin administration reverse maternal separation-induced impairments of prosocial choice behavior. Pharmacology Biochemistry and Behavior *213*. 10.1016/j.pbb.2021.173318.
47. Joushi, S., Taherizadeh, Z., Eghbalian, M., Esmaeilpour, K., and Sheibani, V. (2024). Boosting decision-making in rat models of early-life adversity with environmental enrichment and intranasal oxytocin. Psychoneuroendocrinology *165*. 10.1016/j.psyneuen.2024.107050.
48. Birnie, M.T., Kooiker, C.L., Short, A.K., Bolton, J.L., Chen, Y., and Baram, T.Z. (2020). Plasticity of the Reward Circuitry After Early-Life Adversity: Mechanisms and Significance. Biol Psychiatry *87*, 875-884. 10.1016/j.biopsych.2019.12.018.
49. Tooley, U.A., Bassett, D.S., and Mackey, A.P. (2021). Environmental influences on the pace of brain development. Nat Rev Neurosci *22*, 372-384. 10.1038/s41583-021-00457-5.
50. Kompier, N.F., Keysers, C., Gazzola, V., Lucassen, P.J., and Krugers, H.J. (2019). Early Life Adversity and Adult Social Behavior: Focus on Arginine Vasopressin and Oxytocin as Potential Mediators. Front Behav Neurosci *13*, 143. 10.3389/fnbeh.2019.00143.
51. Calanni, J.S., Dieguez, H.H., Gonzalez Fleitas, M.F., Canepa, E., Berardino, B., Repetto, E.M., Villarreal, A., Dorfman, D., and Rosenstein, R.E. (2023). Early life stress induces visual dysfunction and retinal structural alterations in adult mice. J Neurochem *165*, 362-378. 10.1111/jnc.15752.
52. Luby, J.L., Baram, T.Z., Rogers, C.E., and Barch, D.M. (2020). Neurodevelopmental Optimization after Early-Life Adversity: Cross-Species Studies to Elucidate Sensitive Periods and Brain Mechanisms to Inform Early Intervention. Trends Neurosci *43*, 744-751. 10.1016/j.tins.2020.08.001.
53. Reh, R.K., Dias, B.G., Nelson, C.A., 3rd, Kaufer, D., Werker, J.F., Kolb, B., Levine, J.D., and Hensch, T.K. (2020). Critical period regulation across multiple timescales. Proc Natl Acad Sci U S A *117*, 23242-23251. 10.1073/pnas.1820836117.
54. Sarro, E.C., Wilson, D.A., and Sullivan, R.M. (2014). Maternal regulation of infant brain state. Curr Biol *24*, 1664-1669. 10.1016/j.cub.2014.06.017.
55. Yoshimura, R., Kimura, T., Watanabe, D., and Kiyama, H. (1996). Differential expression of oxytocin

receptor mRNA in the developing rat brain. Neurosci Res *24*, 291-304. 10.1016/0168-0102(95)01003-3.

56. Newmaster, K.T., Nolan, Z.T., Chon, U., Vanselow, D.J., Weit, A.R., Tabbaa, M., Hidema, S., Nishimori, K., Hammock, E.A.D., and Kim, Y. (2020). Quantitative cellular-resolution map of the oxytocin receptor in postnatally developing mouse brains. Nat Commun *11*, 1885. 10.1038/s41467-020-15659-1.
57. Rickenbacher, E., Perry, R.E., Sullivan, R.M., and Moita, M.A. (2017). Freezing suppression by oxytocin in central amygdala allows alternate defensive behaviours and mother-pup interactions. Elife *6*. 10.7554/eLife.24080.
58. Duque-Wilckens, N., Torres, L.Y., Yokoyama, S., Minie, V.A., Tran, A.M., Petkova, S.P., Hao, R., Ramos-Maciel, S., Rios, R.A., Jackson, K., et al. (2020). Extrahypothalamic oxytocin neurons drive stress-induced social vigilance and avoidance. Proc Natl Acad Sci U S A *117*, 26406-26413. 10.1073/pnas.2011890117.
59. Humphreys, K.L., Kircanski, K., Colich, N.L., and Gotlib, I.H. (2016). Attentional avoidance of fearful facial expressions following early life stress is associated with impaired social functioning. J Child Psychol Psychiatry *57*, 1174-1182. 10.1111/jcpp.12607.
60. Hein, T.C., and Monk, C.S. (2017). Research Review: Neural response to threat in children, adolescents, and adults after child maltreatment - a quantitative meta-analysis. J Child Psychol Psychiatry *58*, 222-230. 10.1111/jcpp.12651.
61. Donadon, M.F., Martin-Santos, R., and F, L.O. (2021). Oxytocin effects on the cognition of women with postpartum depression: A randomized, placebo-controlled clinical trial. Prog Neuropsychopharmacol Biol Psychiatry *111*, 110098. 10.1016/j.pnpbp.2020.110098.
62. Zheng, W., Zhu, X.M., Zhang, Q.E., Yang, X.H., Cai, D.B., Li, L., Li, X.B., Ng, C.H., Ungvari, G.S., Ning, Y.P., and Xiang, Y.T. (2019). Adjunctive intranasal oxytocin for schizophrenia: A meta-analysis of randomized, double-blind, placebo-controlled trials. Schizophr Res *206*, 13-20. 10.1016/j.schres.2018.12.007.
63. Sabe, M., Zhao, N., Crippa, A., Strauss, G.P., and Kaiser, S. (2021). Intranasal Oxytocin for Negative Symptoms of Schizophrenia: Systematic Review, Meta-Analysis, and Dose-Response Meta-Analysis of Randomized Controlled Trials. Int J Neuropsychopharmacol *24*, 601-614. 10.1093/ijnp/pyab020.
64. Huang, Y., Huang, X., Ebstein, R.P., and Yu, R. (2021). Intranasal oxytocin in the treatment of autism spectrum disorders: A multilevel meta-analysis. Neurosci Biobehav Rev *122*, 18-27. 10.1016/j.neubiorev.2020.12.028.
65. Sikich, L., Kolevzon, A., King, B.H., McDougle, C.J., Sanders, K.B., Kim, S.J., Spanos, M., Chandrasekhar, T., Trelles, M.D.P., Rockhill, C.M., et al. (2021). Intranasal Oxytocin in Children and Adolescents with Autism Spectrum Disorder. N Engl J Med *385*, 1462-1473. 10.1056/NEJMoa2103583.
66. Winterton, A., Westlye, L.T., Steen, N.E., Andreassen, O.A., and Quintana, D.S. (2021). Improving the precision of intranasal oxytocin research. Nat Hum Behav *5*, 9-18. 10.1038/s41562-020-00996-4.
67. Quintana, D.S., Lischke, A., Grace, S., Scheele, D., Ma, Y., and Becker, B. (2021). Advances in the field of intranasal oxytocin research: lessons learned and future directions for clinical research. Mol Psychiatry *26*, 80-91. 10.1038/s41380-020-00864-7.
68. Shin, S., Pribiag, H., Lilascharoen, V., Knowland, D., Wang, X.Y., and Lim, B.K. (2018). Drd3 Signaling in the Lateral Septum Mediates Early Life Stress-Induced Social Dysfunction. Neuron *97*, 195-208 e196. 10.1016/j.neuron.2017.11.040.

69. Zheng, J.J., Li, S.J., Zhang, X.D., Miao, W.Y., Zhang, D., Yao, H., and Yu, X. (2014). Oxytocin mediates early experience-dependent cross-modal plasticity in the sensory cortices. Nat Neurosci *17*, 391-399. 10.1038/nn.3634.

70. Cetin, A., Komai, S., Eliava, M., Seeburg, P.H., and Osten, P. (2006). Stereotaxic gene delivery in the rodent brain. Nat Protoc *1*, 3166-3173. 10.1038/nprot.2006.450.

71. Zhang, F., Gradinaru, V., Adamantidis, A.R., Durand, R., Airan, R.D., de Lecea, L., and Deisseroth, K. (2010). Optogenetic interrogation of neural circuits: technology for probing mammalian brain structures. Nat Protoc *5*, 439-456. 10.1038/nprot.2009.226.

72. Wang, Y., Pan, Q., Tian, R., Wen, Q., Qin, G., Zhang, D., Chen, L., Zhang, Y., and Zhou, J. (2021). Repeated oxytocin prevents central sensitization by regulating synaptic plasticity via oxytocin receptor in a chronic migraine mouse model. The Journal of Headache and Pain *22*. 10.1186/s10194-021-01299-3.

**Acknowledgements**

We would like to thank Prof. Xiang Yu (School of Life Sciences, Peking University) for providing the OT-Cre (Jackson Laboratory) and $Oxtr^{flox}$ mice (Jackson Laboratory). This work was supported by the National Key R&D Program of China 2022YFE0140400 (to Qingqing Liu), the National Natural Science Foundation of China (32230042 to Liping Wang and 32200828 to Shanping Chen), Financial Support for Outstanding Talents Training Fund in Shenzhen (to Liping Wang), GuangDong Basic and Applied Basic Research Foundation 2023A1515111193 (to Huiying Tan), the CAS Key Laboratory of Brain Connectome and Manipulation (2019DP173024), and Guangdong Provincial Key Laboratory of Brain Connectome and Behavior (2023B1212060055). We sincerely thank the Shenzhen Brain Science Infrastructure for their essential technical support in this study.



**Author contributions**

Liping Wang and Huiying Tan designed the study and the experiments. Huiying Tan, Junying Su, and Shaohua Ma performed the experiments. Shanping Chen analyzed the data. Huiying Tan drafted the manuscript. Qingqing Liu and Xing Yang commented on the manuscript. Liping Wang supervised all aspects of this study.

**Competing interests**

The authors declare no competing interests.

## Figure Legends

### Figure 1. LSD impairs looming-evoked innate defensive behavior in adulthood

**a** Schematic showing the paradigm and strategy used for ELA and observation of looming-evoked innate defensive behavior. Comparison between ESD and control mice of the **b** latency to refuge, **c** representative images of trajectories, **d** distance ratio, **e** speed (black line represents looming stimulus presentation), **f** mean return speed, **g** maximum speed, and **h** time spent in the refuge after looming (n = 48 trials from 17 mice for the control group; n = 57 trials from 20 mice for the ESD group). Comparison between LSD and control mice of the **i** latency to refuge, **j** representative images of trajectories, **k** distance ratio, **l** speed (black line represents looming stimulus presentation), **m** mean return speed, **n** maximum speed, and **o** time spent in the refuge after looming (n = 51 trials from 17 mice for the control group, n = 48 trials from 16 mice for the LSD group). Mann-Whitney U-test, $^{**}p < 0.01$, $^{***}p < 0.001$.



### Figure 2. LSD mice have lower *Oxtr* mRNA expression in the IDSC

**a** Representative immunofluorescence images of OT neurons in the PVN and SON of control (left) and LSD mice (right) (scale bar, 100 μm). **b** Immunofluorescence statistics of no group differences in the number of OT neurons in LSD mice in either the PVN or SON (n = 6 for the control group; n = 6 for the LSD group). **c** No group difference in the total level of *in vitro* OT peptide in the PVN and SON of LSD mice (n = 7 for the control group; n = 7 for the LSD group). **d** No group difference in the total level of OT peptide in the SC of LSD mice (n = 6 for the control group; n = 6 for the

LSD group). **e** Representative FISH image of *c-fos*$^{+}$ cells co-stained with *Oxtr* in the IDSC of control (left) and LSD mice (right) (coronal sections, *c-fos*, green; *Oxtr*, red; DAPI, blue; scale bars, 500 μm and 5 μm). **f** FISH statistics showing decreased *c-fos*$^{+}$ cell density in the IDSC of LSD mice (n = 6 for the control group; n = 6 for the LSD group). **g** FISH statistics showing decreased *Oxtr*$^{+}$ cell density in the IDSC of LSD mice (n = 6 for the control group; n = 6 for the LSD group). **h** FISH statistics showing decreased intensity mean value of *Oxtr* in the *c-fos*$^{+}$ cells of LSD mice (n = 360 cells from 6 mice for the control group; n = 360 cells from 6 mice for the LSD group). Student's *t*-test for **b c d f g**, Mann-Whitney U-test for **h**; $^{**}p < 0.01$, $^{***}p < 0.001$.

**Figure 3. *Oxtr* knockdown in the SC mimics the innate defensive behavior deficit induced by LSD**

**a** Schematic showing the conditional knockdown of *Oxtr* in the SC. **b** Representative images of AAV-hSyn-iCre-GFP expression (GFP, green; DAPI, blue; scale bars, 500 μm and 50 μm). **c** Top: Representative western blots images of OXTR levels in the SC of -/- and +/+ Oxtr$^{flox}$ mice; Bottom: statistical analysis of western blots (n = 4 for both -/- and +/+ groups; Student's *t*-test, $^{*}p < 0.05$). Comparison between Oxtr$^{flox}$ +/+ and -/- mice of the **d** latency to refuge, **e** representative images of trajectories, **f** distance ratio, **g** speed (black line represents looming stimulus presentation), **h** mean return speed, **i** maximum speed, and **j** time spent in the refuge after looming (n = 30 trials from 10 mice for the -/- group, n = 36 trials from 12 mice for the +/+ group; Mann-Whitney U-test, $^{**}p < 0.01$, $^{***}p < 0.001$).

**Figure 4. Activation of oxytocinergic terminals in the IDSC enhances innate defensive behavior**

**a** Schematic showing optogenetic activation of oxytocinergic terminals in the IDSC. **b** Representative image of AAV-hSyn-DIO-ChR2-mCherry expression (ChR2, red; DAPI, blue; scale bars, 500 μm and 50 μm). **c** Representative image showing ChR2-expressing terminals in the IDSC and the position of the fiber track (ChR2, red; DAPI, blue; scale bar, 500 μm and 50 μm). Comparison between ChR2-expressing OT-Cre mice and control mice of the **d** latency to refuge, **e** representative images of trajectories, **f** distance ratio, **g** speed (black line represents looming stimulus presentation), **h** mean return speed, **i** maximum speed, and **j** time spent in the refuge after looming (n = 37 trials from 13 mice for the mCherry group, n = 41 trials from 16 mice for the ChR2 group; Mann-Whitney U-test, $*p < 0.05$, $**p < 0.01$).



**Figure 5. Intranasal OT ameliorates the innate defensive behavior deficit induced by LSD**

Comparison between intranasal OT-treated LSD mice and control mice of the **a** latency to refuge, **b** representative images of trajectories, **c** distance ratio, **d** speed (black line represents looming stimulus presentation), **e** mean return speed, **f** maximum speed, and **g** time spent in the refuge after looming (n = 38 trials from 13 mice for the Ctrl+Saline, n = 39 trials from 13 mice for Ctrl+OT group, n = 42 trials from 14 mice for the LSD+Saline and LSD+OT group; Mann-Whitney U-test, $*p < 0.05$, $**p < 0.01$, $***p < 0.001$).

**Editor Summary**

ELA induced by social deprivation on postnatal days 10–20 impairs looming-evoked innate defensive behaviors via decreased oxytocin receptor mRNA levels in the intermediate and deep layers of the superior colliculus.

**Peer Review Information**

*Communications Biology* thanks Claire-Dominique Walker, Emily C. Wright and the other, anonymous, reviewer(s) for their contribution to the peer review of this work. Primary Handling Editors: Fereshteh Nugent and Benjamin Bessieres. [A peer review file is available.]

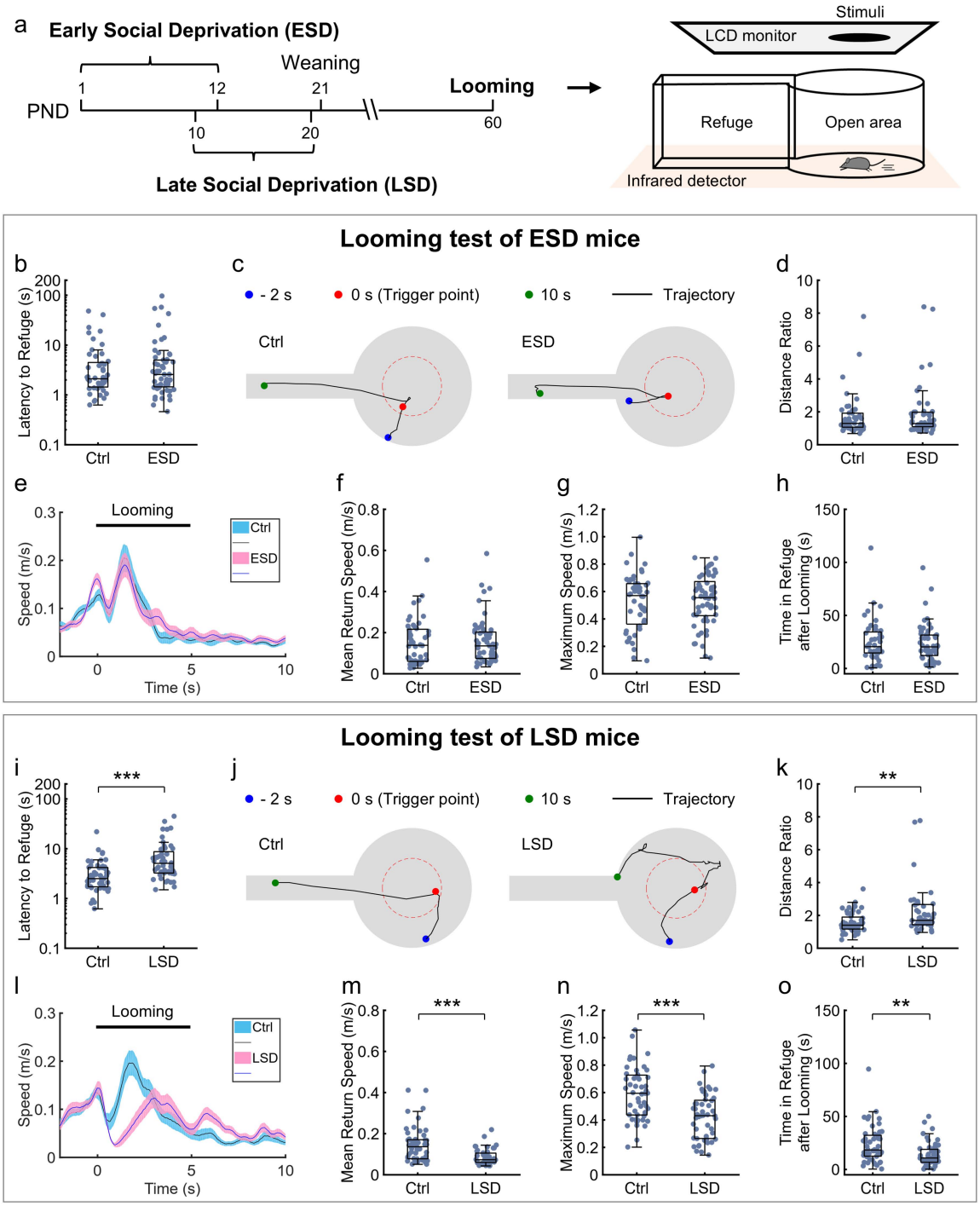
a
Early Social Deprivation (ESD)
Weaning
PND
1
12
21
Looming
60
10
20
Late Social Deprivation (LSD)
Stimuli
LCD monitor
Refuge
Open area
Infrared detector
Looming test of ESD mice
b
Latency to Refuge (s)
Ctrl
ESD
c
- 2 s
0 s (Trigger point)
10 s
Trajectory
Ctrl
ESD
d
Distance Ratio
e
Looming
Speed (m/s)
Time (s)
f
Mean Return Speed (m/s)
g
Maximum Speed (m/s)
h
Time in Refuge after Looming (s)
Looming test of LSD mice
i
***
LSD
j
k
**
l
m
n
o

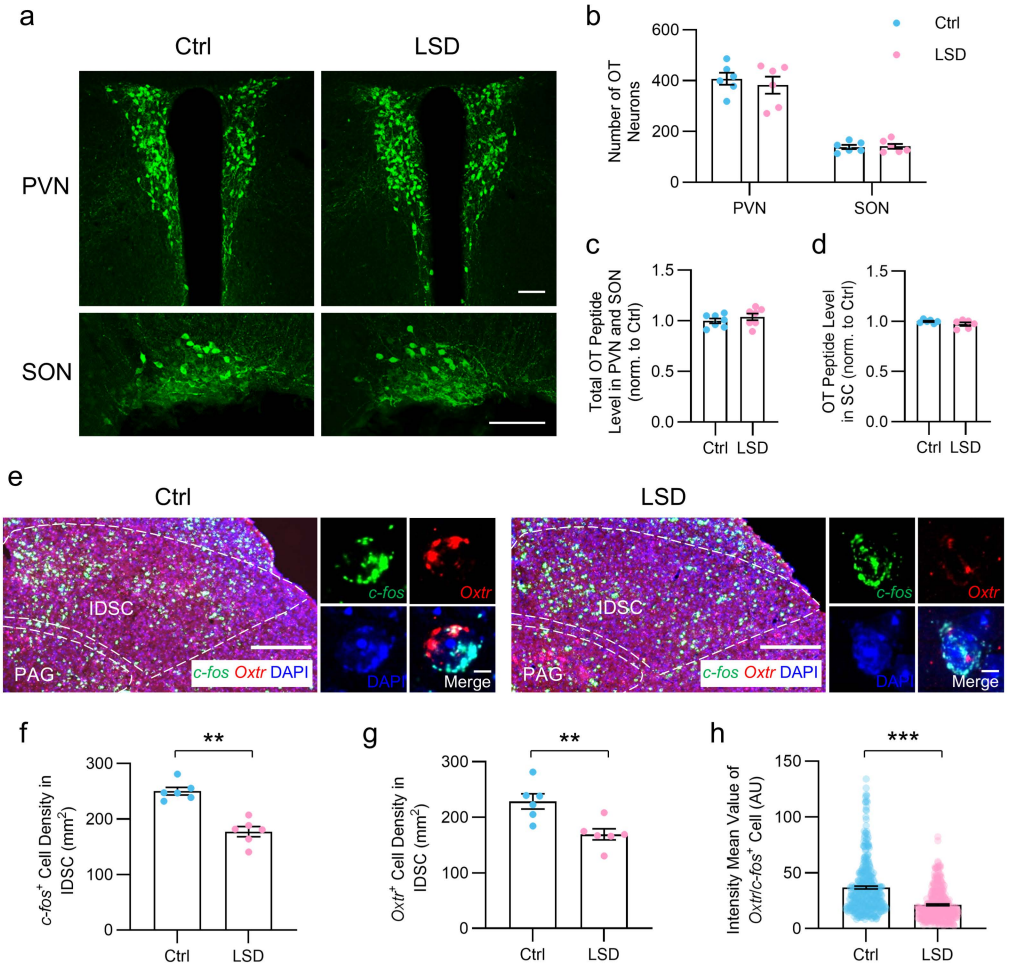
a
Ctrl
LSD
PVN
SON
b
Ctrl
LSD
Number of OT Neurons
600
400
200
0
PVN
SON
c
Total OT Peptide Level in PVN and SON (norm. to Ctrl)
1.5
1.0
0.5
0.0
Ctrl LSD
d
OT Peptide Level in SC (norm. to Ctrl)
1.5
1.0
0.5
0.0
Ctrl LSD
e
Ctrl
LSD
lDSC
PAG
c-fos Oxtr DAPI
c-fos
Oxtr
DAPI
Merge
f
c-fos+ Cell Density in lDSC (mm2)
**
300
200
100
0
Ctrl LSD
g
Oxtr+ Cell Density in lDSC (mm2)
**
300
200
100
0
Ctrl LSD
h
Intensity Mean Value of Oxtr/c-fos+ Cell (AU)
***
150
100
50
0
Ctrl LSD

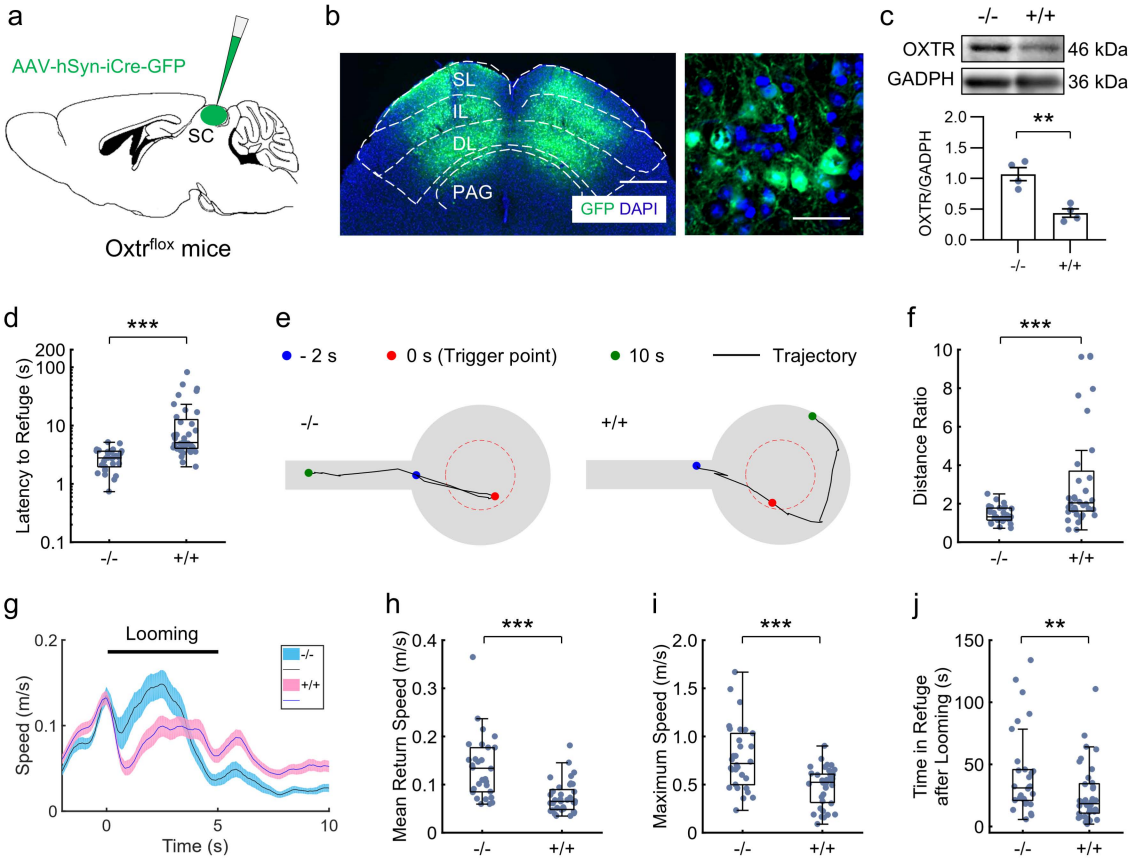
a
AAV-hSyn-iCre-GFP
SC
Oxtr^flox mice
b
SL
IL
DL
PAG
GFP DAPI
c
-/- +/+
OXTR
GADPH
46 kDa
36 kDa
OXTR/GADPH
**
d
***
Latency to Refuge (s)
e
- 2 s
0 s (Trigger point)
10 s
Trajectory
-/-
+/+
f
***
Distance Ratio
g
Looming
Speed (m/s)
Time (s)
h
***
Mean Return Speed (m/s)
i
***
Maximum Speed (m/s)
j
**
Time in Refuge after Looming (s)

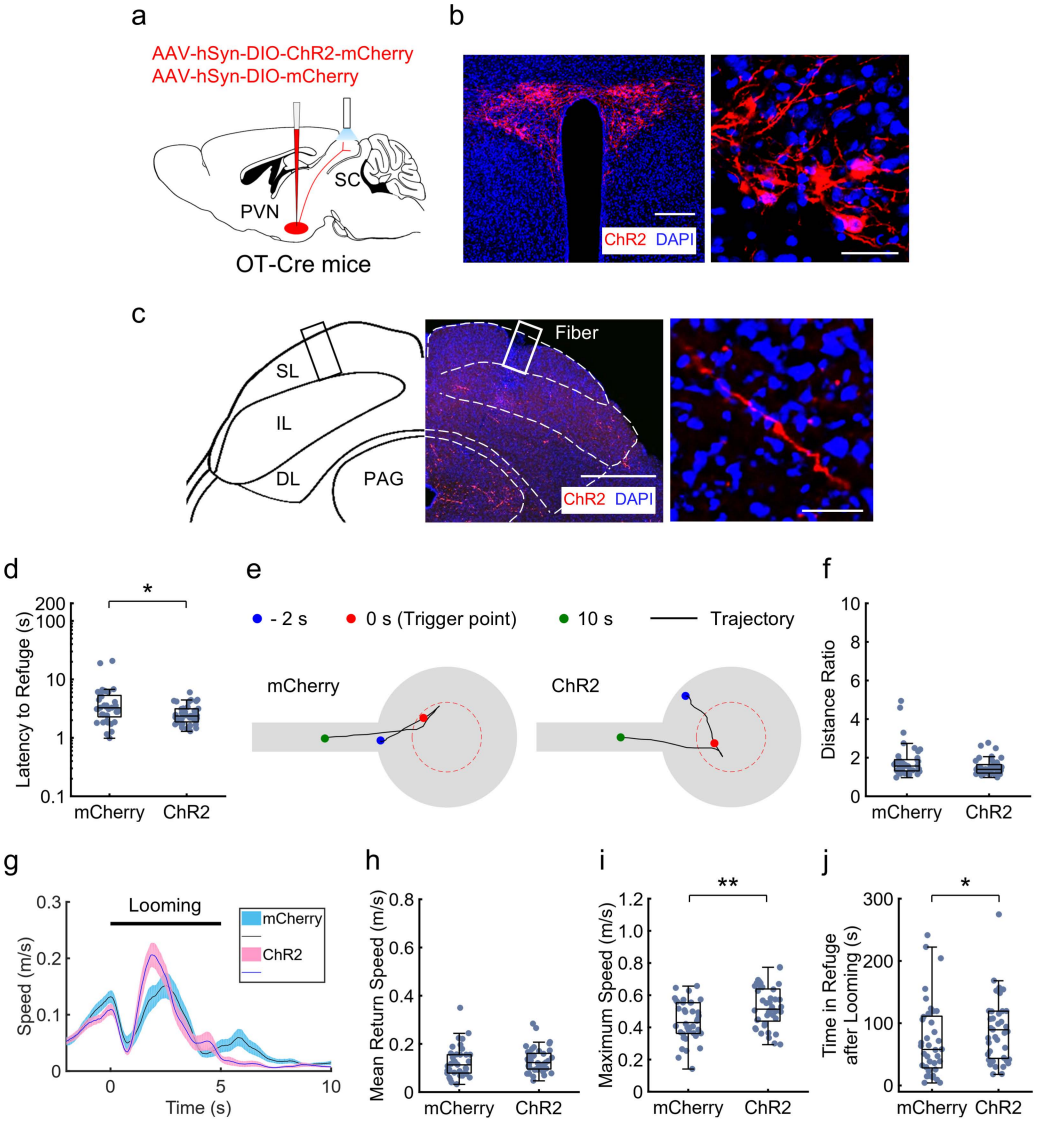
a
AAV-hSyn-DIO-ChR2-mCherry
AAV-hSyn-DIO-mCherry
SC
PVN
OT-Cre mice
b
ChR2 DAPI
c
SL
IL
DL
PAG
Fiber
ChR2 DAPI
d
Latency to Refuge (s)
mCherry
ChR2
e
- 2 s
0 s (Trigger point)
10 s
Trajectory
mCherry
ChR2
f
Distance Ratio
mCherry
ChR2
g
Looming
mCherry
ChR2
Speed (m/s)
Time (s)
h
Mean Return Speed (m/s)
mCherry
ChR2
i
Maximum Speed (m/s)
mCherry
ChR2
j
Time in Refuge after Looming (s)
mCherry
ChR2

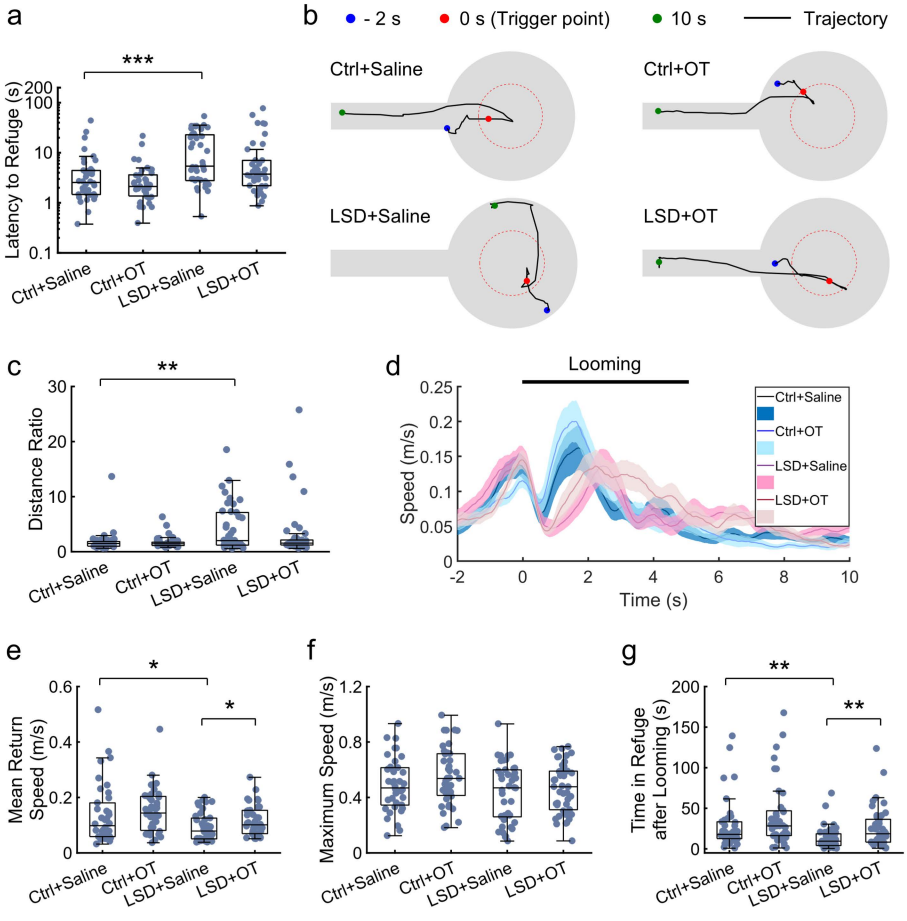
a
***
Latency to Refuge (s)
200
100
10
1
0.1
Ctrl+Saline
Ctrl+OT
LSD+Saline
LSD+OT
b
- 2 s
0 s (Trigger point)
10 s
Trajectory
Ctrl+Saline
Ctrl+OT
LSD+Saline
LSD+OT
c
**
Distance Ratio
30
20
10
0
Ctrl+Saline
Ctrl+OT
LSD+Saline
LSD+OT
d
Looming
Speed (m/s)
0.25
0.2
0.15
0.1
0.05
0
-2
0
2
4
6
8
10
Time (s)
Ctrl+Saline
Ctrl+OT
LSD+Saline
LSD+OT
e
*
*
Mean Return Speed (m/s)
0.6
0.4
0.2
0
Ctrl+Saline
Ctrl+OT
LSD+Saline
LSD+OT
f
Maximum Speed (m/s)
1.2
0.8
0.4
0
Ctrl+Saline
Ctrl+OT
LSD+Saline
LSD+OT
g
**
**
Time in Refuge after Looming (s)
200
150
100
50
0
Ctrl+Saline
Ctrl+OT
LSD+Saline
LSD+OT